

## Performance of DFT Methods in the Calculation of Optical Spectra of TCF-Chromophores

Jan Andzelm,<sup>\*,†</sup> Berend C. Rinderspacher,<sup>†</sup> Adam Rawlett,<sup>†</sup> Joseph Dougherty,<sup>†</sup>  
Roi Baer,<sup>‡</sup> and Niranjana Govind<sup>§</sup>

*U.S. Army Research Laboratory, Aberdeen Proving Ground, Maryland 21005, Institute of Chemistry and Fritz Haber Center for Molecular Dynamics, The Hebrew University of Jerusalem, Jerusalem 91904, Israel, and William R. Wiley Environmental Molecular Sciences Laboratory, Pacific Northwest National Laboratory, Richland, Washington 99352*

Received May 8, 2009

**Abstract:** We present electronic structure calculations of the ultraviolet/visible (UV–vis) spectra of highly active push–pull chromophores containing the tricyanofuran (TCF) acceptor group. In particular, we have applied the recently developed long-range corrected Baer-Neuhauser-Livshits (BNL) exchange–correlation functional. The performance of this functional compares favorably with other density functional theory (DFT) approaches, including the CAM-B3LYP functional. The accuracy of UV–vis results for these molecules is best at low values of attenuation parameters ( $\gamma$ ) for both BNL and CAM-B3LYP functionals. The optimal value of  $\gamma$  is different for the charge-transfer (CT) and  $\pi$ – $\pi^*$  excitations. The BNL and PBE0 exchange correlation functionals capture the CT states particularly well, while the  $\pi$ – $\pi^*$  excitations are less accurate and system dependent. Chromophore conformations, which considerably affect the molecular hyperpolarizability, do not significantly influence the UV–vis spectra on average. As expected, the color of chromophores is a sensitive function of modifications to its conjugated framework and is not significantly affected by increasing aliphatic chain length linking a chromophore to a polymer. For selected push–pull aryl-chromophores, we find a significant dependence of absorption spectra on the strength of diphenylaminophenyl donors.

### I. Introduction

Organic chromophores possessing a high degree of  $\pi$ -conjugation are ideal materials for advanced electronic and photonic applications including optical information processing, photovoltaic cells, photodynamic therapy agents, and many other applications.<sup>1</sup> These properties are due to the stable, macrocyclic, conjugated network of  $\pi$ -electrons, which lead to high electrical polarizabilities and rapid nonlinear optical responses (NLO) of the charge density to the applied intense electromagnetic fields. The optical spectra and NLO properties of chromophores may be conveniently

modified *via* a change of molecular architecture, substituent groups, and substitution patterns.<sup>2–7</sup>

The need to understand the relationship between chemical structure and NLO properties at the molecular level has led to the exploration of various electron-donor and electron-acceptor end-groups linked through  $\pi$ -bridges of various natures and lengths. One of the most successful NLO systems combines the 2-dicyanomethyl-3-cyano-4,5,5-trimethyl-2,5-dihydrofuran acceptor end-group, often referred to as “tricyanofuran” (TCF), with substituted amine donor end-groups. The  $\pi$ -linkage may include thienylvinylene (FTC)<sup>3</sup> and tetraene (CLD)<sup>4</sup> type bridges.

These push–pull chromophores exhibit superior NLO properties, characterized by a large hyperpolarizability ( $\beta$ ) values and good thermal and chemical stabilities. Devising efficient electro-optical (EO) materials that also have good

\* Corresponding author e-mail: jandzelm@arl.army.mil.

<sup>†</sup> U.S. Army Research Laboratory, Aberdeen Proving Ground.

<sup>‡</sup> The Hebrew University of Jerusalem.

<sup>§</sup> Pacific Northwest National Laboratory.

optical transparency represents a considerable development dilemma. For instance, the transparent chromophores in a visible yellow spectral range are typically small molecules with a low EO response, while molecules possessing large  $\beta$ -values are frequently opaque or, at best, have small windows of visibility. The visibility window in these NLO frameworks is generally bracketed by two kinds of electronic transitions.<sup>2–7</sup> The blue-shifted transition is a local excitation of  $\pi$ - $\pi^*$  character, while the red-shifted transition is characterized by a significant intramolecular charge-transfer (CT). The CT peak is typically the maximum absorption peak ( $\lambda_{\max}$ ), while the  $\pi$ - $\pi^*$  transition has a much lower oscillator strength and could be denoted as  $\lambda_{\max-1}$ . An increase in the  $\beta$ -value due to a change in end-groups is usually accompanied by a red-shift of the  $\lambda_{\max}$  peak. The optimal chromophores, which are transparent in the visible spectrum, would have a red-shifted  $\lambda_{\max}$ -peak, while the  $\lambda_{\max-1}$ -peak should be blue-shifted to open a large visibility window. In this work, we assess the accuracy of computational methods in predicting both the  $\lambda_{\max}$ - and  $\lambda_{\max-1}$ -peaks of optical absorption spectra. A reliable computational method, if available, would allow the prediction of both the position and intensity of either peak with a small, consistent error. This would facilitate the formulation of a relationship between molecular structure and the UV-vis absorption spectra of chromophores and contribute to the design of chromophores which are transparent in the visible.

Due to the almost limitless optimization space of chromophore structures, computational tools are increasingly being used to assist experimental efforts in designing optimal chromophores. By far the most often used computational approaches are semiempirical and DFT methods. The semiempirical computational methods, such as INDO/CIS, are fast and accurate for chromophores similar to systems for which the method was parametrized.<sup>8</sup>

DFT offers the best compromise between accuracy and computational performance for typical chromophores of about 100 atoms. The electronic spectra are often calculated using time-dependent density-functional theory (TD-DFT)<sup>9,10</sup> and numerous successes of this technique have been recently reviewed.<sup>11</sup>

Recent papers on visible absorption spectra of numerous organic dyes<sup>12</sup> found that the DFT method at the PBE0 level delivers overall the best estimates of  $\lambda_{\max}$  values. In the case of push-pull  $\pi$ -conjugated chromophores, it is well-known that the conventional exchange-correlation potentials of DFT fail to predict accurately optical properties.<sup>13</sup> Unacceptably large errors were reported for chromophores with increasing chain lengths of the conjugated framework.<sup>14,15</sup> The failure of TD-DFT calculations has been associated with the incorrect asymptotic behavior of typical exchange-correlation (XC) potentials. These approximate XC potentials do not correctly treat self-repulsion, which leads to the so-called self-interaction error (SIE).<sup>11</sup> As a result, the excited states of dyes, in particular the charge-transfer (CT) of chromophores, are poorly described.<sup>13,16,17</sup> Recently, a new class of DFT functionals has been proposed, which includes a growing fraction of “exact” exchange as the distance increases.<sup>18–24</sup> These long-range corrected (LC) functionals

have been found to provide improved correlation between calculated and experimental optical properties of several dyes.<sup>12,24</sup> The recently proposed BNL functional,<sup>21,23</sup> which falls into this LC-class, is of particular interest for studying push-pull dyes because it has been shown to reproduce exactly the CT excitation for intermolecular complexes.<sup>23</sup> The full long-range cancelation of self-repulsion in BNL restores the long-range effective potential  $1/r$  and also allows an improved CT excitation description for intermolecular complexes. In this paper, we report the implementation of the BNL method in the parallel NWChem program package.<sup>25</sup> The performance of the BNL method will be compared with other DFT approaches, in particular with the CAM-B3LYP functional.<sup>12,22</sup>

The focus of this research is push-pull chromophores with large  $\beta$ -values for which accurate experimental UV-vis spectra are available. We present representative results for four types of molecules: 2-dicyanomethylen-3-cyano-4-[2-[E-(4-N,N-di(2-acetoxyethyl)-amino)-phenylene-(3,4-dibutyl)-thien-5]-E-vinyl]-5,5-dimethyl-2,5-dihydrofuran<sup>3,5</sup> (denoted FTC), CLD,<sup>4,5</sup> recently synthesized, highly efficient chromophores<sup>6</sup> based on the (4-diaryloamino) phenyl electron donors and 2-dicyanomethylen-3-cyano-4-methyl-5-phenyl-5-trifluoro-methyl-2,5-dihydrofuran (CF<sub>3</sub>-TCF) electron acceptors, and the TCV chromophore with a strong acceptor (tricyanovinyl) and donor (dimethylamine).<sup>26</sup> This selection allows us to evaluate and validate the theoretical methods for calculating absorption spectra of this important class of molecules.

Several studies have been published critically comparing the performance of various computational methods for chromophores with TCF acceptors. The most comprehensive comparison of Hartree-Fock (HF), INDO, and DFT methods in calculations of dipole moments, polarizabilities, and  $\beta$ -values was published by Isborn et al.<sup>27</sup> They found that the relative merits of molecules are consistently predictable with every method. However, no optical absorption spectra were evaluated in this work. The effect of conformation and isomerization on NLO properties of the FTC chromophore have been reported by Kinnibrugh et al.<sup>28</sup> The  $\beta$ -values change significantly even for nearly degenerate conformers. However, the effect of isomerization on the absorption spectra of FTC was not investigated. The INDO method was recently used to compare properties of several chromophores with strong nitrile-based acceptor end-groups and various modifications of the  $\pi$ -bridge.<sup>29,30</sup> The trends in  $\beta$ - and  $\lambda_{\max}$ -values have been correlated with modifications of the chemical structure. The errors in absolute values of  $\lambda_{\max}$  as calculated with the INDO approximation can reach 150 nm or more, which is almost as large as the entire visibility window of interest. Moreover, no  $\lambda_{\max-1}$ -peak was calculated, thus making it difficult to evaluate the applicability of the INDO method in predicting the transparency window of such chromophores.

This paper is organized as follows. First, we will describe the implementation of the BNL method in the NWChem program and verify the sensitivity of the method to the choice of technical parameters, such as basis set or model of solvation. We will then verify the performance of standard

DFT functionals for chromophores with the TCF motif and study the dependence of absorption spectra on the choice of low lying conformers of FTC and CLD. This will allow us to select the most stable conformer for a detailed study of comparing the performance of the DFT-LC method for several chromophores with TCF-type acceptors. We will judge the applicability of DFT-LC functionals in predicting the visibility window by comparing positions of both the  $\lambda_{\max}$ - and  $\lambda_{\max-1}$ -absorption peaks and their corresponding oscillator strengths to experimental data. Finally, the BNL method will be applied to study the effect of varying substituents in models of CF3-TCF-type chromophores on the respective optical spectra. The optimized structures are provided as Supporting Information.

## II. Computational Methodology

The structures of all molecular systems were calculated using the Gaussian03 program.<sup>31</sup> The B3LYP exchange-correlation functional and the 6-31(d,p) basis set were used in the gas phase calculations.<sup>31–34</sup> The geometry optimization in a solvent was done using the PCM model as implemented in Gaussian03.<sup>35</sup> The vertical excitation energies were calculated using the time-dependent DFT (TDDFT)<sup>10,36</sup> module implemented in the NWChem computational chemistry package<sup>25</sup> developed at the Pacific Northwest National Laboratory. This program allows us to compare the performance of several long-range corrected (LC) DFT approaches<sup>21–23</sup> as well as other typical DFT exchange-correlation functionals, which is one of the main goals of this paper. To simulate the effect of the solvent on the excitation energies, we have used the COSMO solvation model<sup>37</sup> implemented in NWChem.

Three classes of DFT functionals are investigated here. The first class consists of the fundamental local density (LDA) and generalized-gradient (GGA) approximations<sup>38</sup> represented by SVWN and PBE,<sup>39</sup> respectively. LDA and GGA depend on the electron density and its gradient, respectively.<sup>38</sup> The second class is comprised of three hybrid methods, B3LYP,<sup>32–34</sup> PBE0,<sup>40</sup> and BH&H.<sup>41</sup> In all these hybrids, the percentage of Hartree–Fock exchange is constant at each point in space, and it amounts to 20, 25, and 50% of HF exchange for B3LYP, PBE0, and BH&H, respectively. The hybrid functionals yield quite accurate transition energies for many organic dyes; however, they poorly describe charge-transfer states that dominate the  $\lambda_{\max}$ -transitions of the molecules studied in this paper. The most successful strategy used to solve this problem involves the use of the LC DFT functionals.<sup>18–24</sup> These functionals include a growing fraction of Hartree–Fock exchange when the interelectronic distance increases, thus effectively limiting the dominant self-interaction error at large distances. This procedure, originally suggested by Savin,<sup>18</sup> has been further extended resulting in several implementations of LC-DFT functionals. The essence of these functionals lies in partitioning the Coulomb operator into long- and short-range components<sup>22,24</sup> in an Ewald-like fashion as

$$\frac{1}{r} = \frac{1}{r} \{1 - [\alpha + \beta \text{erf}(\gamma r)]\} + \frac{1}{r} [\alpha + \beta \text{erf}(\gamma r)] \quad (1)$$

where  $\gamma$  is the attenuation or range-separation parameter, while  $\alpha$  and  $\beta$  define the contributions of the Hartree–Fock exchange. With this, the exchange energy,  $E_x$ , can be partitioned into short- and long-range components, respectively

$$E_x = E_x(\text{short}) + E_x(\text{long}) \quad (2)$$

The short-range part of the exchange is treated with traditional DFT, while the long-range component is treated with “exact” exchange. A crucial issue in the construction of these functionals is the choice of parameters  $\alpha$ ,  $\beta$ , and  $\gamma$ . The parameters  $\alpha$  and  $\beta$  satisfy the relations  $0 \leq \alpha \leq 1$ ,  $0 \leq \beta \leq 1$ , and  $0 \leq \alpha + \beta \leq 1$ .<sup>20–24</sup> In this work, we have used the CAM-B3LYP functional of Handy and co-workers, which applies the Coulomb attenuation method to B3LYP.<sup>22</sup> We have used two parametrizations of CAM-B3LYP, the original one with  $\alpha = 0.19$ ,  $\beta = 0.46$  and a modified one with  $\alpha = 0.19$  and  $\beta = 0.81$ .<sup>22</sup> The first parametrization yields  $\alpha + \beta = 0.65$ , so no exact asymptote of the exchange potential is reached. The second parametrization yields  $\alpha + \beta = 1$  indicating that the  $E_x(\text{long})$  term, asymptotically (at  $r \rightarrow \infty$ ) is equal to Hartree–Fock exchange.

In the BNL LC approach<sup>21,23</sup> the electron repulsion is also separated into long- and short-range parts according to eq 1; however, the parameters are set to  $\alpha = 0$  and  $\beta = 1$ . Therefore, the short-range part is treated with traditional DFT, while the long-range component, unlike the CAM-B3LYP functional described above, attains the “exact” exchange value only in the asymptotic limit. In the BNL functional, the exchange-correlation energy per particle is separated into  $\gamma$ -dependent exchange and correlation parts respectively as follows

$$\varepsilon_{xc}^\gamma(n) = \varepsilon_x^\gamma(n) + \varepsilon_c^\gamma(n) \quad (3)$$

where  $n$  represents the density. The exchange energy per particle is presented in Savin’s form,<sup>18</sup> where  $q = (\gamma)/(k_f)$  and  $k_f$  is the local Fermi vector at the given density  $n$ . The exchange and correlation energies are represented as

$$\varepsilon_c^\gamma(n, |\nabla n|) = \varepsilon_c^{LYP}(n, |\nabla n|) - w\varepsilon_x^\gamma(n) \quad (4)$$

where the major part of the correlation energy has been represented with the GGA functional LYP.<sup>32</sup> It has been found that subtracting a small piece of the Savin exchange (eq 4) with a small mixing factor  $w$  improves the overall performance of the functional.<sup>23</sup> It can be shown that the theory becomes more HF-like for large  $\gamma$  and behaves more local DFT-like for small  $\gamma$ . A crucial issue in the construction of LC functionals is the choice of  $\gamma$ . It has been shown<sup>23</sup> that this parameter can be optimized using an extensive molecular training set, but recent calculations<sup>42</sup> have revealed that this parameter is in fact system-dependent. The value  $\gamma = 0.5$  was used in the original paper, while  $\gamma$  as small as  $\sim 0.1$  has been recommended for some metallic systems.<sup>42</sup> In this study, we performed further validation of this parameter on the molecular systems considered in this paper.



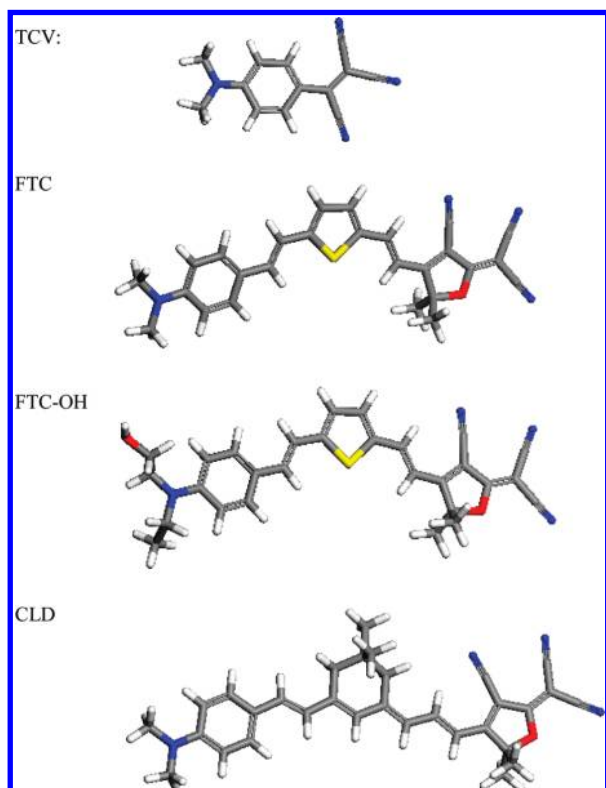


**Figure 1.** The B3LYP/6-31G\*\* optimized structures of TCV, FTC, FTC–OH, and CLD chromophores.

To estimate the vertical excitation energies, we have used the TD-DFT approach.<sup>9,10</sup> TD-DFT is an extension of DFT in which electronic excitations are calculated as the poles of the electron density response.<sup>9,10</sup> We also tested the Tamm-Dancoff approximation,<sup>43</sup> as it is computationally more efficient than solving the complete TD-DFT equations. We found a systematic blue-shift of spectra and decided not to use this approximation. We have frozen the atom-like core orbitals in TD-DFT calculations.

Since the long-range part of LC-functionals has to be calculated explicitly, the 2-electron integrals have to be considered with care. In particular, the exchange interactions have to be treated separately from the pure Coulomb interactions because the attenuation just affects the exchange. We have implemented two approaches to deal with this. The first approach utilizes the well-known Dunlap<sup>44</sup> charge fitting method for the pure Coulomb interactions, whereas the exchange contribution (including the attenuation) is treated in the conventional manner. The second approach involves calculating directly all the exchange integrals. Our charge fitting approach is implemented along the lines of the von Arnim and Ahlrichs implementation.<sup>45</sup> The Coulomb contribution with this approach is evaluated with 3-center integrals. The in-core strategy in NWChem for storing all the 3-center, 2-electron integrals in memory also allows for a much faster evaluation of the Coulomb contribution compared with disk-based or direct approaches. We have used the DFT DGauss Coulomb fitting basis<sup>46</sup> for the charge fitting on all the atoms.

The effect of basis set expansion on UV–vis spectra was studied for the TCV molecule presented in Figure 1. Table 1 shows  $\lambda_{\max}$ - and  $\lambda_{\max-1}$ -transitions and corresponding

oscillator strengths obtained for basis sets of increasing size. Both hybrid and Coulomb attenuation functionals were tested. In order to compare the BNL and CAM-B3LYP functionals, common parameters,  $\gamma = 0.33$  and  $\alpha + \beta = 1$ , were used for both functionals. For the CAM-B3LYP calculations we have used  $\alpha = 0.19$ ,  $\beta = 0.81$  and for the LC-BNL calculations we have used  $\alpha = 0$ ,  $\beta = 1$ , respectively. The extension of basis sets leads to red-shifted spectra by less than 20 nm in the case of the  $\lambda_{\max}$ -peak and less than 10 nm for the  $\lambda_{\max-1}$ -peak. The oscillator strengths are more sensitive to the basis set choice, particularly for the  $\lambda_{\max-1}$ -peak of the CAM-B3LYP method. We also tested the accuracy of fitting functions by comparing results with those obtained using a direct method that does not employ fitting functions. No significant deterioration of results was observed due to the fitting. In the case of very large chromophores, we have used the smaller 6-31G\* basis set as it represents the best compromise between computational efficiency and accuracy.

Predicting the effect of a solvent on absorption spectra is a difficult task as, in principle, it requires consideration of both a fast, electronic and a slow, orientational relaxation response of a solvent.<sup>47,48</sup> Solvents of interest have typically very low dielectric constants, and we assume that excitation energies are not too sensitive to the choice of the solvation model. In this work, we have considered the “conductor-like screening model” COSMO as implemented in the NWChem program. In this model, the solute interacts with the solvent represented by a dielectric continuum model.<sup>37,48</sup> The solute molecule is embedded into a cavity surrounded by a dielectric continuum of permittivity  $\epsilon$ . The dielectric screening energies for a given geometry scale as  $(\epsilon - 1)/(\epsilon + x)$  with the dielectric permittivity  $\epsilon$  of the screening medium, where  $x$  is in the range of 0–2. The scaling  $x(= 0)$  was used,<sup>49</sup> and it was confirmed that  $x(= 1/2)$  shifts  $\lambda_{\max}$  by less than 5 nm, even for the chloroform solvent with a very low dielectric. We have tested several techniques of building the COSMO cavity considering different sets of radii<sup>48,49</sup> and tessellation of the unit sphere as well as octahedral and icosahedral representations of the cavity surface.<sup>25</sup> The absorption spectra of the TCV, FTC, and CLD molecules appear to be little affected, and, therefore, the NWChem default COSMO parameters were used throughout this study. Finally, we have tested the effect of structural changes due to the presence of solvent on the absorption spectra and found a small red shift of less than 5 nm for both peaks. In summary, we expect that the red-shift of absorption spectra due to the choice of basis set or solvent model does not exceed 20 nm. We further assume that the possible discrepancy with respect to experimental values larger than 30 nm is caused by the inaccuracy of the particular DFT functional.

The accuracy of the absorption spectra calculations could be improved by using highly correlated ab initio approaches such as CCSD or CAS-PT2 methods. The CAS-PT2 method could account for the multiconfigurational nature of the chromophore’s wave function. It is known that CAS-PT2 underestimates slightly excitation energies and needs an empirical correction.<sup>50</sup> Furthermore, the application of CAS-

**Table 1.** UV-vis Spectra and Oscillator Strength ( $f$ ) of TCV Calculated at the BNL, B3LYP, and CAM-B3LYP Levels for Various Basis Sets<sup>b</sup>

basis set	BNL		B3LYP		CAM-B3LYP	
	$\lambda_{\max}$ (f)	$\lambda_{\max-1}$ (f)	$\lambda_{\max}$ (f)	$\lambda_{\max-1}$ (f)	$\lambda_{\max}$ (f)	$\lambda_{\max-1}$ (f)
6-31G*	396(0.81)	237(0.21)	451(0.66)	289(0.13)	412(0.78)	255(0.10)
6-31G**	396(0.81)	238(0.21)	452(0.65)	290(0.13)	412(0.77)	255(0.09)
6-311G*	402(0.80)	240(0.19)	456(0.65)	292(0.12)	417(0.77)	257(0.06)
6-311G* <sup>a</sup>	402(0.80)	240(0.20)	456(0.65)	292(0.12)	417(0.77)	258(0.06)
6-31+G*	411(0.83)	243(0.21)	462(0.67)	295(0.12)	423(0.79)	253(0.15)
6-311+G*	412(0.81)	243(0.20)	464(0.66)	295(0.12)	424(0.77)	255(0.16)
6-311++G**	412(0.81)	245(0.15)	464(0.66)	295(0.12)	425(0.77)	256(0.17)

<sup>a</sup> Direct calculations without density fitting functions. <sup>b</sup> The  $\lambda_{\max}$ ,  $\lambda_{\max-1}$  (in nm), and oscillator strengths ( $f$ ) values are provided. Calculations were done using the COSMO solvation model, assuming the 1,4-dichloroethane solvent.

PT2 becomes prohibitively expensive with sufficiently large active spaces.<sup>12,50</sup> Therefore as a compromise of computational expense and accuracy, we have not performed CAS-PT2 calculations for the TCF-chromophores considered in this paper.

### III. Results and Discussion

**A. Validation of DFT Methodology.** The structures of chromophores with the TCF motif used to validate the performance of DFT functionals are presented in Figure 1. These are the lowest energy structures as calculated at the B3LYP/6-31G(d,p) level of theory in the gas phase. The experimental UV-vis spectra for these molecules in a solvent environment are available and, therefore, the 1,2-dichloroethane solvent was considered for TCV, while cyclohexanone and tetrahydrofuran solvents were used in FTC and CLD chromophore calculations, respectively, for comparison with experiment. The values of the dielectric constants used in the continuous electrostatic models were 10.3, 18.2, and 7.6, respectively. The spectra for FTC and CLD chromophores were measured with a hydroxyl-diethylamine donor instead of the simplified dimethylamine shown in Figure 1.<sup>5</sup> We have performed calculations with the diethyl donor and its hydroxyl derivative (FTC-OH chromophore displayed in Figure 1) finding that the main features of the spectra, such as absorption peak ( $\lambda_{\max}$ ), were shifted by less than 10 nm with the increased size of a donor group.

Table 2 includes TD-DFT results of vertical excitation spectra including  $\lambda_{\max}$ ,  $\lambda_{\max-1}$ , and corresponding oscillator strengths at various levels of DFT theory. The Hartree-Fock, hybrid DFT functionals (B3LYP, PBE0, B3LYP), gradient corrected DFT (PBE), and the simplest, density-dependent, SVWN functionals were used. The experimental oscillator strengths were obtained by fitting two Gaussians to the two major peaks in the experimental spectrum. The ratio of the area under each Gaussian was used to estimate the respective relative oscillator strengths.<sup>51</sup> This is a crude approximation of the transition strength; nevertheless, it can shed light on the relative importance of transitions and width of the visibility window.

As expected, the accuracy of results in matching the experimental data depends strongly on the method used. The PBE and SVWN methods reproduce within 30 nm major absorption peaks but quite poorly the relative oscillator strengths of the TCV chromophore. However, this level of theory fails completely for the larger FTC and CLD systems.

**Table 2.** Absorption Spectra ( $\lambda_{\max}$  and  $\lambda_{\max-1}$  in nm) and Oscillator Strengths ( $f$ ) of TCV, FTC, and CLD for Various DFT Functionals<sup>a</sup>

functional	$\lambda_{\max}$	$f_{\max}$	$\lambda_{\max-1}$	$f_{\max-1}$	rel. $f^b$
TCV					
PBE	504	0.55	328	0.14	0.25
PBE0	451	0.70	285	0.12	0.17
BHLYP	411	0.82	254	0.12	0.14
B3LYP	462	0.67	294	0.12	0.18
SVWN	509	0.55	330	0.14	0.25
HF	355	0.96	222	0.16	0.17
expt	518		292		0.08
FTC					
PBE	766	1.07	541	0.83	0.78
PBE0	637	1.54	439	0.49	0.32
BHLYP	514	2.40	350	0.23	0.10
B3LYP	663	1.43	458	0.57	0.40
SVWN	785	1.01	544	0.86	0.85
HF	458	1.90	295	0.14	0.07
expt	650		400		0.26
CLD					
PBE	728	1.45	555	0.91	0.63
PBE0	621	2.18	450	0.39	0.18
BHLYP	548	2.55	372	0.05	0.02
B3LYP	639	2.07	468	0.47	0.23
SVWN	735	1.44	559	0.92	0.64
HF	462	2.75	238	0.20	0.07
expt	660		420		0.04

<sup>a</sup> COSMO/6-31+G\*\*/B3LYP/6-31G\*\*. <sup>b</sup> The relative value of oscillator strengths  $f_{\lambda_{\max}}/f_{\lambda_{\max-1}}$ .

The hybrid functionals, which yield erroneously blue-shifted absorption peaks in the case of TCV, perform much better for the FTC and CLD chromophores. The accuracy improves with decreasing amount of Hartree-Fock exchange in the hybrid functional. The B3LYP method shows improved values for  $\lambda_{\max}$ , while the values for  $\lambda_{\max-1}$  are significantly red-shifted. The PBE0 method could be recommended for FTC and CLD systems as the best compromise. It both underestimates the  $\lambda_{\max}$  peak and overestimates  $\lambda_{\max-1}$  by about 40 nm. The relative values of the oscillator strengths are predicted to be too high particularly for the CLD chromophore. The use of PBE0 was recently recommended for calculations of the  $\pi-\pi^*$  transitions for numerous organic dyes.<sup>12b</sup>

We now turn to evaluate the performance of Coulomb attenuation functionals, CAM-B3LYP and BNL. Tables 3 and 4 display absorption spectra and oscillator strengths of TCV, FTC, and CLD as a function of the attenuation parameter,  $\gamma$ . Regardless of the type of LC-DFT functional,

**Table 3.** UV-vis Spectra and Oscillator Strength ( $f$ ) of TCV, FTC, and CLD Chromophores (Figure 1) Calculated at the CAM-B3LYP Level with Various Attenuation Parameters,  $\gamma^a$ 

method ( $\gamma$ )	TCV		FTC		CLD	
	$\lambda_{\max}$ (f)	$\lambda_{\max-1}$ (f)	$\lambda_{\max}$ (f)	$\lambda_{\max-1}$ (f)	$\lambda_{\max}$ (f)	$\lambda_{\max-1}$ (f)
experiment <sup>b</sup>	518(1.00)	292(0.08)	650(1.00)	400(0.26)	660(1.00)	420(0.04)
$\gamma^c$						
0.01	464(0.67)	295(0.12)	657(1.61)	456(0.81)	642(2.04)	472(0.49)
0.05	462(0.67)	293(0.12)	632(1.79)	437(0.63)	627(2.20)	452(0.32)
0.10	453(0.70)	283(0.13)	583(2.08)	392(0.29)	597(2.36)	410(0.10)
0.15	438(0.74)	267(0.16)	547(2.21)	333(0.19)	572(2.46)	317(0.14)
0.20	424(0.78)	256(0.20)	522(2.25)	313(0.21)	553(2.45)	300(0.15)
0.33	399(0.85)	235(0.24)	485(2.29)	280(0.20)	519(2.48)	274(0.14)
$\gamma^d$						
0.01	464(0.67)	295(0.12)	657(1.61)	456(0.81)	642(2.04)	472(0.49)
0.05	462(0.67)	293(0.12)	642(1.71)	445(0.70)	627(2.19)	452(0.32)
0.10	457(0.68)	288(0.11)	609(1.92)	418(0.49)	614(2.26)	434(0.23)
0.15	449(0.71)	280(0.09)	584(2.04)	395(0.33)	596(2.35)	413(0.13)
0.20	440(0.74)	266(0.10)	565(2.11)	378(0.23)	582(2.41)	327(0.13)
0.33	423(0.79)	253(0.14)	528(2.21)	320(0.19)		

<sup>a</sup>  $\lambda_{\max}$  and  $\lambda_{\max-1}$  (nm) with significant values of oscillator strength are reported. The most stable conformer was used within the COSMO environment. The 6-31+G\* basis set was used. <sup>b</sup> Relative values of oscillator strengths are reported. <sup>c</sup> CAM-B3LYP parametrization  $\alpha/\beta$  with  $\alpha = 0.19$ ,  $\beta = 0.81$  is used. <sup>d</sup> CAM-B3LYP parametrization  $\alpha/\beta$  with  $\alpha = 0.19$ ,  $\beta = 0.46$  is used.

**Table 4.** UV-vis Spectra and Oscillator Strength of TCV, FTC, and CLD Chromophores (Figure 1) Calculated at the BNL Level with Various Attenuation Parameters,  $\gamma^a$ 

method ( $\gamma$ )	TCV		FTC		CLD	
	$\lambda_{\max}$ (f)	$\lambda_{\max-1}$ (f)	$\lambda_{\max}$ (f)	$\lambda_{\max-1}$ (f)	$\lambda_{\max}$ (f)	$\lambda_{\max-1}$ (f)
experiment <sup>b</sup>	518(1.00)	292(0.08)	650(1.00)	400(0.26)	660(1.00)	420(0.04)
0.01	510(0.54)	330(0.13)	781(0.97)	536(1.04)	732(1.47)	561(0.83)
0.05	507(0.55)	326(0.12)	722(1.25)	511(0.84)	700(1.79)	528(0.58)
0.10	492(0.59)	309(0.13)	641(1.68)	444(0.48)	649(2.20)	462(0.21)
0.15	469(0.65)	291(0.14)	584(1.89)	396(0.26)	608(2.35)	416(0.06)
0.20	448(0.71)	272(0.14)	546(1.98)	365(0.22)	579(2.39)	386(0.01)
0.33	411(0.83)	243(0.21)	490(2.25)	293(0.24)	531(2.41)	345(0.04)

<sup>a</sup> Structure, basis set, and solvation model are the same as in Table 3. <sup>b</sup> Relative values of oscillator strengths are reported.

we observe a red-shift of the spectra with decreasing  $\gamma$ . This is consistent with the results obtained using standard DFT functionals, as reported in Table 2. Decrease in  $\gamma$  diminishes the role of Hartree–Fock exchange, which accounts for a significant red-shift of spectra for DFT functionals such as PBE. For the same value of  $\gamma$ , the spectra are more red-shifted for BNL compared to the CAM-B3LYP functional. For BNL, one can identify the common value of  $\gamma$  approximately equal to 0.1, that results in a  $\lambda_{\max}$  close, within 20 nm, to the experimental values for all test molecules. In the case of the FTC molecule, both CAM-B3LYP and BNL perform reasonably well, if  $\gamma$  close to 0.05 and 0.1 is used, respectively. The positions of the  $\lambda_{\max}$ -peaks, and the relative strengths of peaks are well reproduced; however, the  $\lambda_{\max-1}$ -peak is red-shifted by ca. 40 nm. The sensitivity to  $\gamma$ -values of absorption spectra for various systems was already reported in the literature.<sup>42,52–55</sup> The results of Table 3 and 4 suggest also a strategy of using different values of  $\gamma$  to calculate various excitations. In the case of BNL, the optimal position of the  $\lambda_{\max}$ -peak can be obtained using  $\gamma = 0.1$ , while the larger value of  $\gamma = 0.15$  may be needed to improve the prediction for the  $\lambda_{\max-1}$ -peak. This would however worsen the description of the relative strength of both peaks for the FTC molecule while improving it for the CLD chromophore.

Recently the performance of DFT functionals was analyzed, and a diagnostic test was proposed to predict the

accuracy of excitation energies.<sup>56</sup> This test was based on the spatial overlap of occupied and virtual orbitals,  $\Lambda$ . One of the molecules studied in that paper, DMABN, is similar to the TCV molecule studied by us, the difference being a cyano acceptor vs the TCF acceptor, respectively. In the case of the PBE functional, the DMABN molecule exhibits a large value of  $\Lambda$  and also quite an accurate description of the CT excited state.<sup>56</sup> We did not implement the diagnostic test in this paper; however, following conclusions by Peach et al.<sup>56</sup> we can predict that less accurate results of excitation energies for FTC and CLD molecules indicate a small  $\Lambda$  value, while excellent results for TCV molecule are likely related to a large  $\Lambda$  (see Table 2).

The absorption spectra results could perhaps be further improved by considering statistical corrections that were recently applied for the LC-functionals in calculations of  $\pi-\pi^*$ <sup>12b</sup> and  $n-\pi^*$  excitations.<sup>57</sup>

To analyze the nature of the discussed  $\lambda_{\max}$  and  $\lambda_{\max-1}$  states, the transition orbitals are frequently displayed, and their contributions to the excitation energies as found from the TD-DFT calculations are discussed.<sup>13,14,28</sup> As expected, the excitation at  $\lambda_{\max}$  has a charge-transfer character as it is dominated by transitions from HOMO to LUMO orbitals of the chromophore. The HOMO orbital is predominantly localized on a donor site of the chromophore, while the LUMO orbital occupies the acceptor site. The HOMO→LUMO transition gives rise to a well-known intramolecular charge-

**Table 5.** Analysis of the Electronic Excitations (CT and  $\pi-\pi^*$  Transitions) for the FTC Chromophore Calculated at the BNL Level with Various Attenuation Parameters,  $\gamma^a$ 

method ( $\gamma$ )	CT		$\gamma-\gamma^*$		
	H $\rightarrow$ L	H-1 $\rightarrow$ L	H-1 $\rightarrow$ L	H $\rightarrow$ L+1	H-L <sup>b</sup>
0.01	0.96	0.24	0.77	0.54	1.33
0.05	0.99	0.13	0.82	0.53	2.36
0.10	0.99	0.10	0.89	0.37	3.26
0.15	0.95	0.25	0.91	0.08	3.96
0.20	0.90	0.34	0.86	0.25	4.45
0.33	0.84	0.44	0.68	0.57	5.34

<sup>a</sup> The absolute values of weights for two major orbital transitions of each excitation are shown. Computational parameters are the same as in Table 4. <sup>b</sup> The HOMO(H) - LUMO(L) gap in eV.

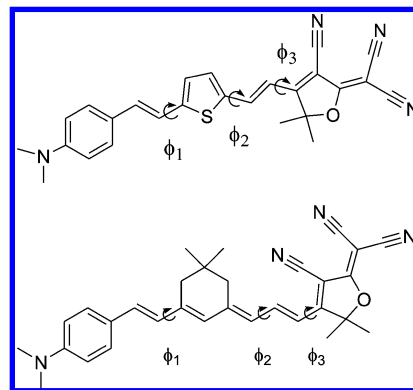
transfer state.<sup>11,13,14</sup> The excitation at  $\lambda_{\max-1}$  can be recognized as a  $\pi-\pi^*$  transition, as it involves orbitals below the HOMO and above the LUMO that span the entire framework of the chromophore. We have analyzed orbital contributions to the electronic transitions for the FTC chromophore calculated using the BNL approach for various attenuation parameters,  $\gamma$ . The absolute values of weights and the character of major orbital transitions are presented in Table 5. This confirms that the  $\lambda_{\max}$ -peak can be interpreted as a charge-transfer peak because the major contribution comes from the HOMO to LUMO excitation. Similarly the  $\lambda_{\max-1}$ -peak involves  $\pi$ -electron excitations, and it is dominated by the HOMO-1 to LUMO excitation. It is interesting to note that the  $\lambda_{\max}$ -peak has increased charge-transfer character around  $\gamma = 0.1$ , as the contribution of the HOMO-1 $\rightarrow$ LUMO transition shows a minimum at this value. Similarly the  $\lambda_{\max-1}$ -peak has the strongest  $\pi-\pi^*$  character about  $\gamma = 0.15$ . This strengthening of the charge-transfer and  $\pi-\pi^*$  characters coincides with an improved performance of the BNL functional in predicting  $\lambda_{\max}$ - and  $\lambda_{\max-1}$ -peaks, respectively. As is evident from Table 4, the excitation energies are consistently red-shifted with decrease of the attenuation parameter. This corresponds to closing the HOMO-LUMO gap as shown in Table 5.

In summary, assuming a target accuracy of 30 nm in the prediction of the most important  $\lambda_{\max}$ -transition, we can recommend the BNL method with attenuation parameter  $\gamma = 0.1$  for systems studied in this work. For the FTC and CLD chromophores, the hybrid functionals B3LYP and PBE0 as well as CAM-B3LYP with  $\gamma = 0.05$  would also yield the  $\lambda_{\max}$ -transition within our target accuracy.

### B. Absorption Spectra of FTC and CLD Conformers.

Extended molecules such as FTC and CLD have several rotatable single bonds, which lead to the existence of conformers with low relative energies. The manifold of rotational isomers of the FTC chromophore was recently studied by Kinnibrugh et al.<sup>29</sup> The authors found relatively low barriers for rotations along the single bonds, indicating that the lifetime of a given rotamer is on the order of 2.5 ms, thus making it quite plausible that several rotamers coexist in the gas phase as well as in a low-viscosity solution.

The eight low-energy conformers of each molecule were optimized, and a significant dependence of NLO properties on the conformer's structure was observed.<sup>29</sup> The values of the hyperpolarizability projected on the axis of the dipole moment can vary by a factor of 2 between close-lying

**Figure 2.** Definition of dihedral angles used to study conformations of FTC and CLD chromophores.

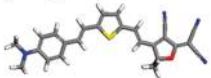
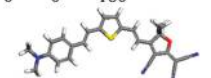
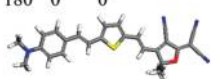
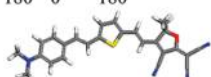
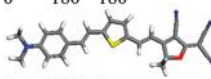
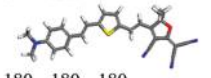
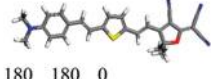
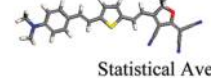
conformers. The effect of the conformational space on the UV-vis spectra has not been considered until now.

We have optimized the structures of the eight conformers that can be created by rotations around the single bonds as presented in Figure 2. The structures of the conformers were optimized at the B3LYP/6-31G\*\* level of theory in the gas phase (G), and the absorption spectra were calculated in the presence of solvent (S) modeled at the COSMO level of theory. Tables 6 and 7 present results of absorption spectra for FTC and CLD conformers, respectively. The energy differences between conformers, in kcal/mol, are presented in the gas phase (G) as well as in the solvent, S. Both the G and S calculations utilize the gas-phase-optimized structure. The effect of solvent can change the ordering of conformers separated by less than 2 kcal/mol for both the FTC and CLD chromophores. The structures of the gas-phase chromophores are close in energy, within 3 and 8 kcal/mol for FTC and CLD systems, respectively. The presence of solvent changes these values by 1 kcal/mol at most. Since the solvent field is much stronger in the case of FTC than CLD, we have optimized the structures of FTC at the B3LYP/6-31G\*\* level with the PCM solvation model. The inclusion of the PCM solvation model in the geometry optimization changes the order of the conformers and overall spreads the distribution of the eight FTC isomers to 5.7 kcal/mol. This solvent-optimized geometry however has only a minor effect on the absorption spectra, and while the statistical average of  $\lambda_{\max-1}$  appears to be red-shifted by about 11 kcal/mol, the average  $\lambda_{\max}$  value is virtually unchanged at 652 nm. We can hence adopt a computationally much simpler strategy of using the gas-phase-optimized geometry to calculate the absorption spectra in the solvent environment of the COSMO model.

Results in Tables 6 and 7 indicate that the Boltzmann-weighted root-mean-square deviation over all conformers was less than 10 nm for  $\lambda_{\max}$  and less than 5 nm for  $\lambda_{\max-1}$ . While the addition of solvation effects shifts the spectra appropriately, this does not change the influence of the conformation, neither at the gas phase nor at the solvated geometry. It is therefore acceptable to use the lowest-energy geometry in the gas phase with solvation effects for the computation of spectra. The results obtained for the lowest-energy conformer are within 12 nm or better of the statistical average of all conformers. Equally important is the analysis of the relative strength of the transitions as measured by the



**Table 6.** Optimized Gas-Phase Geometries and Optical Spectra for FTC<sup>a,b,c,d</sup>

$\phi_1$	$\phi_2$	$\phi_3$	$\Delta E^b$	$\Delta E^c$	$\lambda_{\max}$	$f_{\max}$	$\lambda_{\max-1}$	$f_{\max-1}$
0	0	0	0.0	0.44	661	1.45	457	0.55
								
0	0	180	0.41	0.55	659	1.35	454	0.55
								
180	0	0	0.86	3.77	625	1.71	449	0.50
								
180	0	180	1.43	0	644	1.55	452	0.67
								
0	180	180	1.74	1.82	670	1.55	456	0.70
								
0	180	0	1.99	1.21	668	1.47	461	0.51
								
180	180	180	2.55	2.51	652	1.63	452	0.79
								
180	180	0	2.79	1.18	653	1.55	456	0.66
								
Statistical Average					649	1.49	467	0.62
Statistical Deviation					9	0.08	2.9	0.06
Relative f						1.00	0.41±0.06	
Experiment					650	1.00	400	0.26

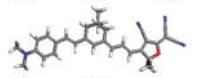
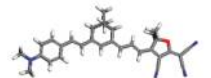
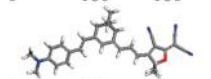
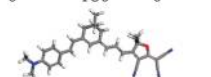
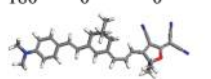
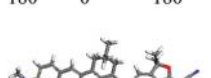
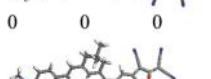
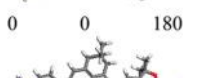
<sup>a</sup>  $\lambda_{\max}$ ,  $\lambda_{\max-1}$ , and corresponding oscillator strengths (f) from B3LYP/COSMO/6-31+G\*\*/B3LYP/6-31G\*\*. <sup>b</sup> Energy differences from B3LYP/6-31G\*\*/B3LYP/6-31G\*\*. <sup>c</sup> Energy differences from B3LYP/COSMO/6-31G\*\*/B3LYP/6-31G\*\*. <sup>d</sup> Dihedral angles are defined in Figure 2.

ratio of oscillator strengths. In the case of the lowest-energy conformers this ratio is within 10% and 15% of the statistical average for the FTC and CLD chromophores, respectively.

Overall, the B3LYP functional performs very well in reproducing the position of the charge-transfer  $\lambda_{\max}$ -peak, while yielding the  $\lambda_{\max-1}$ -peak significantly red-shifted by about 50 nm, that is outside of our error expectation of about 30 nm. The utility of the B3LYP functional is further diminished considering that the intensity of the  $\pi-\pi^*$  peak appears to be erroneously much stronger than needed. Thus the visibility window, as predicted by the B3LYP method, is much narrower than observed in experiment. The conclusion of this section is transferable to other DFT calculations including the BNL functional. Kinnibrugh et al.<sup>29</sup> recently have found that the distribution of values of hyperpolarizability tensors for FTC conformers is fairly similar regardless of the B3LYP or PBE method used. Therefore, we expect that the optical properties of the lowest energy conformer are representative of the entire ensemble of chromophore conformers, unless external fields, such as an electric field, are imposed.

**C. Absorption Spectra of Diarylamino-phenyl-Containing Chromophores.** The highly efficient and thermally stable NLO chromophores based on (4-diaryloamino) phenyl

**Table 7.** Optimized Gas-Phase Geometries and Optical Spectra for CLD<sup>a,b,c,d</sup>

$\phi_1$	$\phi_2$	$\phi_3$	$\Delta E^b$	$\Delta E^c$	$\lambda_{\max}$	$f_{\max}$	$\lambda_{\max-1}$	$f_{\max-1}$
180	180	180	0.0	0.27	639	2.07	468	0.47
								
180	180	0	1.11	0	649	1.95	463	0.83
								
0	180	180	2.46	3.25	640	1.92	473	0.40
								
0	180	0	3.50	2.27	640	1.90	469	0.58
								
180	0	0	4.84	6.01	653	1.92	469	0.52
								
180	0	180	5.91	5.54	650	1.97	470	0.52
								
0	0	0	7.34	6.93	650	1.86	473	0.44
								
0	0	180	8.31	6.55	645	1.92	474	0.37
								
Statistical Average					646	1.94	470	0.52
Statistical Deviation.					6	0.06	4	0.14
Relative f						1.0	0.26±0.08	
Experiment					660		420	

<sup>a</sup>  $\lambda_{\max}$ ,  $\lambda_{\max-1}$ , and corresponding oscillator strengths (f) from B3LYP/COSMO/6-31+G\*\*/B3LYP/6-31G\*\*. <sup>b</sup> Energy differences from B3LYP/6-31G\*\*/B3LYP/6-31G\*\*. <sup>c</sup> Energy differences from B3LYP/COSMO/6-31G\*\*/B3LYP/6-31G\*\*. <sup>d</sup> Dihedral angles are defined in Figure 2.

donors have been recently synthesized and the absorption spectra have been published,<sup>6</sup> thus providing an opportunity to validate further the BNL technique. These chromophores contain a very strong electron-withdrawing acceptor, 2-dicyanomethylen-3-cyano-4-methyl-5-phenyl-5-trifluoromethyl-2,5-dihydrofuran (CF<sub>3</sub>-TCF), linked to the donor *via* a  $\pi$ -conjugated bridge containing thiophene or isophore rings. In this work, we evaluate the performance of DFT in predicting spectra of thiophene-based chromophores (A1-A4) as presented in Figure 3 using the protocol derived in the previous sections. The geometry was optimized in the gas phase at the B3LYP/6-31G\*\* level of theory and was subsequently used in TD-DFT calculations at the BNL/COSMO/6-31G\* level of theory. A solvent with a dielectric constant of 4.9  $\epsilon_0$  corresponding to chloroform was used in the COSMO simulations. Following the recommendation of section A, the three best DFT functionals (BNL, B3LYP, and PBE0) for the FTC-type chromophores were used. The calculated vertical excitation energies are presented in Table 8. The BNL functional was applied with the attenuation parameter set to 0.1. Inspection of Table 8 confirms that both



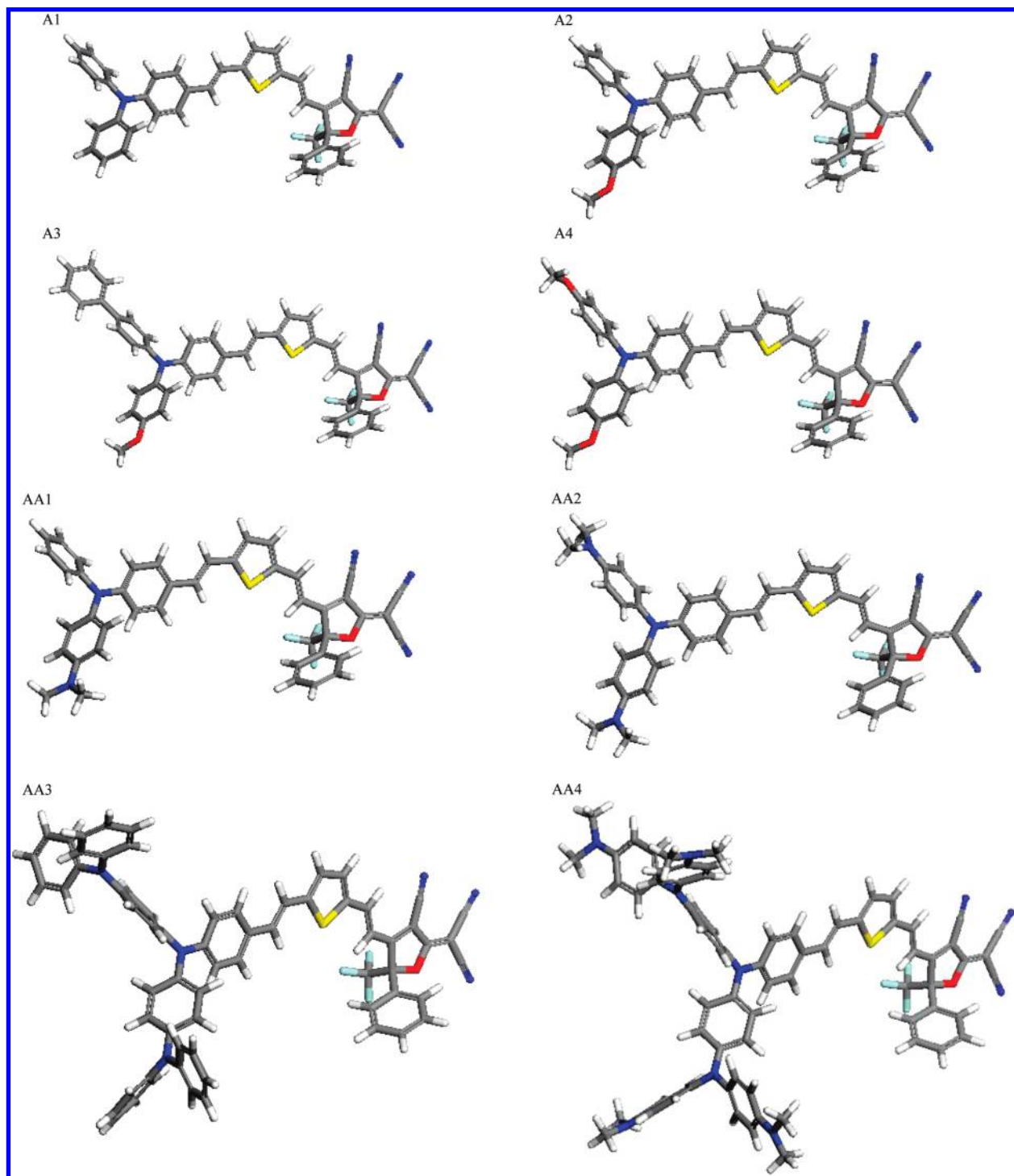


**Figure 3.** The B3LYP/6-31G\*\* optimized structure of A1-A4 and AA1-AA4 chromophores.

PBE0 and BNL predict the positions of excitation levels, exceptionally well. Unlike the parent FTC molecule, the  $\lambda_{\max-1}$ -excitations are also very well reproduced. Analysis of the relative intensity of the two main excitations reveals that BNL is superior. This has important consequences in the selection of an appropriate method to predict reliably the visibility window of chromophores.

The  $\lambda_{\max}$ - and  $\lambda_{\max-1}$ -transitions can be identified as a charge-transfer- and a  $\pi-\pi^*$ -transition, since the major contributions are from HOMO $\rightarrow$ LUMO and HOMO-1 $\rightarrow$ LUMO excitations, respectively. A systematic red-shift of transitions can be seen in Table 8 that correlates well with

increasing donor strength. With two additional methoxy groups on the donor,  $\lambda_{\max}$  of A4 is shifted by about 50 nm compared to the A1 structure, which exhibits  $\lambda_{\max}$  at 685 nm. This shift as calculated at the BNL level matches very well experimental observation. The increased charge transfer to the  $\pi$ -conjugated bridge of the chromophore can also be correlated with the increased dipole moment from 25.3 to 30.7 D for the A1 and A4 chromophores, respectively. We have optimized further the donating strength of aminophenyl donors and replaced the methoxy groups by methyloamino groups resulting in structures AA1-AA4 as shown in Figure 3. The UV-vis spectra for the three highest excitations with

**Table 8.** UV-vis Spectra and Oscillator Strength of A1-A4 and Chromophores (Figure 3) Calculated at the B3LYP, PBE0, and BNL Levels and Compared with Experimental Results from Ref 6

	$\lambda_{\max}$ ( $f_{\max}$ )	$\lambda_{\max-1}$ ( $f_{\max-1}$ )	$f_{\max-1}/f_{\max}$
A1			
B3LYP	729(1.22)	500(0.88)	0.72
PBE0	687(1.39)	479(0.76)	0.55
BNL	685(1.53)	475(0.50)	0.32
expt	694	485	0.06
A2			
B3LYP	750(1.21)	514(0.92)	0.76
PBE0	708(1.34)	492(0.82)	0.61
BNL	706(1.51)	486(0.57)	0.38
expt	717	500	0.20
A3			
B3LYP	762(1.20)	519(1.02)	0.85
PBE0	716(1.35)	497(0.91)	0.67
BNL	708(1.59)	489(0.61)	0.38
expt	721	500	0.20
A4			
B3LYP	782(1.19)	525(0.98)	0.82
PBE0	737(1.32)	504(0.89)	0.67
BNL	735(1.49)	497(0.64)	0.42
expt	745	500	0.35

**Table 9.** UV-vis Spectra, Oscillator Strength, and Dipole Moments ( $\mu$ ) of AA1-AA4, Chromophores (Figure 3) and Analysis of Electronic Excitations As Calculated at the BNL Level

chromophore	$\lambda_{\max}$ ( $f_{\max}$ ) <sup>a</sup>	$\lambda_{\max-1}$ ( $f_{\max-1}$ )	$\lambda_{\max-2}$ ( $f_{\max-2}$ )	$\mu$
AA1	763(1.22)	545(0.70) <sup>b</sup>	460(0.23) <sup>c</sup>	29.3
AA2	842(1.24)	547(0.79) <sup>c</sup>	544(0.12) <sup>b</sup>	33.9
AA3	776(1.29)	544(0.80) <sup>c</sup>	453(0.22) <sup>d</sup>	27.4
AA4	957(0.88)	640(1.15) <sup>c</sup>	498(0.32) <sup>d</sup>	36.2

<sup>a</sup> Major contribution from the HOMO(H)→LUMO(L) transition. <sup>b</sup> H-1→L. <sup>c</sup> H-2→L. <sup>d</sup> H-3→L, H→L+1.

significant oscillator strengths are presented in Table 9. We observe a significant red-shift of the charge-transfer peak that correlates fairly well with the increased dipole moment of the chromophore. The  $\lambda_{\max}$ -peak arises from HOMO→LUMO transitions and therefore can be interpreted as a charge-transfer transition. In the case of AA4, this is no longer the strongest excitation; nevertheless, we maintain the notation for consistency.  $\lambda_{\max-1}$  is due to a  $\pi$ - $\pi^*$ -transition, as it arises from HOMO-1→LUMO excitations for AA1 and HOMO-2→LUMO for other chromophores.  $\lambda_{\max-2}$  for AA3 and AA4 arises from orbitals below the HOMO level and also involves higher virtual orbitals. The  $\pi$ - $\pi^*$ -excitation is the strongest peak for the AA4 chromophore.

In conclusion, by adjusting the donor strength, we succeeded in pushing the charge-transfer peak to the far-red. However, excitations of  $\pi$ - $\pi^*$ -character are strengthened and even further red-shifted. Therefore, it is unlikely that the modifications of the CF3-FTC chromophore architecture by increasing the donor strength will increase the transparency window in the visible. Further study involving modifications of acceptor and substitutions in the conjugated bridge are being carried out and will be reported in the future.

## IV. Conclusions

We have assessed the efficiency of several DFT functionals for reproducing the experimental UV-vis charge-transfer and  $\pi$ - $\pi^*$  absorption wavelengths of a set of push-pull chromophores containing the “tricyanofuran” (TCF) motif in the acceptor. These chromophores are thermally stable and exhibit excellent nonlinear optical properties.

Since our focus is to investigate optical transparency in the visible, the positions of major absorption peaks and their relative strengths are discussed in this work. We find that the PBE or SVWN give very poor estimates of absorption peaks, while hybrid functionals such as B3LYP and particularly PBE0 provide more consistent results for the molecules studied here. The performance of PBE0 is even more impressive considering its lack of empirical parametrization.

The long-range DFT Coulomb attenuation functionals offer a possibility to improve the accuracy of computed spectra by adjusting the attenuation parameter,  $\gamma$ . We have implemented the recently developed long-range-corrected Baer-Neuhausser-Livshits (BNL) exchange-correlation functional in the NWChem program and compared its performance with the popular CAM-B3LYP functional. The accuracy of UV-vis results is best at low values of attenuation parameters ( $\gamma$ ) for both the BNL and CAM-B3LYP functionals. We observed that the optimal value of  $\gamma$  is different for the charge-transfer- and  $\pi$ - $\pi^*$ -excitations. We recommend the BNL (with  $\gamma = 0.1$ ) and PBE0 methods as they capture the charge-transfer states particularly well, although the  $\pi$ - $\pi^*$ -excitations are computed less accurately depending on the specific system. This recommendation of the BNL method is valid for TCF chromophores and may not be applicable to other types of push-pull chromophores. In fact, transferability of both CAM-B3LYP and BNL methods is somewhat limited as their performance depends strongly on the value of attenuation parameter. “A priori” prediction of optimal value of  $\gamma$  for the BNL method remains an outstanding problem that only recently has been addressed, e.g. in calculations of intermolecular charge transfer complexes.<sup>42</sup> The value of  $\gamma$  optimized for the excitation energies is typically a bad choice when used for ground-state properties.<sup>23,53,54</sup> Recently Rohrdanz et al.<sup>55</sup> proposed a unified LC-DFT-type functional that shows promising accuracy in both ground and excited state calculations. Performance of this functional in calculations for the TCF chromophores is as yet unknown.

One of the goals of this work is to validate a practical, computational approach to predict spectra of chromophores in a realistic polymer environment. Chromophores may have side-chains linking a molecule to a polymer and exhibit numerous conformational states close in energy. Overall, a dielectric environment with a low dielectric constant may be expected. We confirm that the color of chromophores is not significantly affected by increasing aliphatic chain length linking a chromophore to a polymer. Unlike the strong dependence of the molecular hyperpolarizability on various conformers, we find that the optical absorption spectra are much less sensitive. The Boltzman statistical average of absorption peaks for various conformers is within  $\sim 10$  nm of the spectra of the most stable conformer. This allows us

to formulate an approximate, yet fairly accurate and practical approach. The lowest-energy-conformer is identified and its geometry optimized utilizing B3LYP in the gas phase, and the spectra are subsequently calculated using TD-DFT with an appropriate solvation model. The procedure outlined in this paper based on the BNL ( $\gamma = 0.1$ ) functional in the COSMO solvent environment yields consistently good results with the largest error found to be  $\sim 40$  nm in the case of  $\pi-\pi^*$ -excitations.

We have studied the effect of increased donor strength on absorption spectra for the CF3-FTC chromophore architecture with amino-phenyl donors. Substituting methoxy groups with methylamino groups, we succeeded in pushing the charge-transfer peak to the far-red. However, excitations of  $\pi-\pi^*$ -character are strengthened and even further red-shifted. Therefore, it is unlikely that the modifications of the CF3-FTC chromophore architecture by increasing the donor strength alone will increase the transparency window in the visible.

**Acknowledgment.** We would like to thank Geoffrey A. Lindsay, Andrew P. Chafin and Timothy M. Pritchett for helpful discussions.

**Supporting Information Available:** Optimized structures. This material is available free of charge via the Internet at <http://pubs.acs.org>.

## References

- Andrekson, P. A.; Westlund, M. *Laser Photonics Rev.* **2007**, *1*, 231–248.
- Pereverzev, Y. V.; Gunnerson, K. N.; Prezhdo, O. V.; Sullivan, P. A.; Liao, Y.; Olbricht, B. C.; Akelaitis, A. J.; Jen, A. K.-Y.; Dalton, L. R. *J. Phys. Chem. C* **2008**, *112*, 4355–4363, and references therein.
- Robinson, B. H.; Dalton, L. R.; Harper, A. W.; Ren, A.; Wang, F.; Zhang, Z.; Todorova, G.; Lee, M.; Aniszfeld, R.; Garner, S.; Chen, A.; Steier, W. H.; Houbrecht, S.; Persoons, A.; Ledoux, I.; Zyss, J.; Jen, A. K.-Y. *Chem. Phys.* **1999**, *245*, 35–50.
- (a) Zhang, C.; Dalton, L. R.; Oh, M.-C.; Zhang, H.; Steier, W. H. *Chem. Mater.* **2001**, *13* (9), 3043. (b) Jen, A.; Luo, J.; Kim, T.-D.; Chen, B.; Jang, S.-H.; Kang, J.-W.; Tucker, N. M.; Hau, S.; Tian, Y.; Ka, J.-W.; Haller, M.; Liao, Y.; Robinson, B.; Dalton, L.; Herman, W. *Proc. SPIE* **2005**, *5935*, 593506–1.
- Guenther, A. J.; Wright, M. E.; Fallis, S.; Lindsay, G. A.; Petteys, B. J.; Yandek, G. R.; Zang, D. Y.; Sanghadasa, M.; Ashley, P. R. *Proc. SPIE* **2006**, *6331*, 63310M–1.
- Cheng, Y.-J.; Luo, J.; Hau, S.; Bale, D. H.; Kim, T.-D.; Shi, Z.; Lao, D. B.; Tucker, N. M.; Tian, Y.; Dalton, L. R.; Reid, P. J.; Jen, A. K.-Y. *Chem. Mater.* **2007**, *19*, 1154–1163.
- Davies, J. A.; Elangovan, A.; Sullivan, P. A.; Olbricht, B. C.; Bale, D. H.; Ewy, T. R.; Isborn, C. M.; Eichinger, B. E.; Robinson, B. H.; Reid, P. J.; Li, X.; Dalton, L. R. *J. Am. Chem. Soc.* **2008**, *130*, 10565.
- Kanis, D. R.; Ratner, M. A.; Marks, T. J. *Chem. Rev.* **1994**, *94*, 195–242.
- Gross, E. K. U.; Dobson, J. F.; Petersilka, M. *Density Functional Theory*; Springer: Berlin, 1996; Vol. 181.
- Casida, M. E.; Jamorski, C.; Casida, K. C.; Salahub, D. R. *J. Chem. Phys.* **1998**, *108*, 4439.
- Dreuw, A.; Head-Gordon, M. *Chem. Rev.* **2005**, *105*, 4009–4037.
- (a) Jacquemin, D.; Perpète, E.; Scalmani, G.; Frisch, M. J.; Kobayashi, R.; Adamo, C. *J. Chem. Phys.* **2007**, *126*, 144105. (b) Jacquemin, D.; Perpète, E.; Scuseria, G. E.; Ciofini, I.; Adamo, C. *J. Chem. Theory Comput.* **2008**, *4*, 123–135.
- Magyar, R. J.; Tretiak, S. *J. Chem. Theory Comput.* **2007**, *3*, 976–987.
- Champagne, B.; Perpète, E. A.; Jacquemin, D.; Gisbergen, S. J. A.; Baerends, E.-J.; Soubra-Ghaoui, C.; Robins, K. A.; Kirtman, B. *J. Phys. Chem. A* **2000**, *104*, 4755–4763.
- Dierksen; Grimme, S. *J. Phys. Chem. A* **2004**, *108*, 10225.
- Dreuw, A.; Head-Gordon, M. *J. Am. Chem. Soc.* **2004**, *126*, 4007–4016.
- Tozer, D. J. *J. Chem. Phys.* **2003**, *119*, 12697–12699.
- Savin, A. *Recent Advances in Density Functional Methods: Part I*; Chong, D. P., Ed.; World Scientific: Singapore, 1995; p 129.
- Leininger, T.; Stoll, H.; Werner, H.-J.; Savin, A. *Chem. Phys. Lett.* **1997**, *275*, 151.
- Iikura, H.; Tsuneda, T.; Yanai, T.; Hirao, K. *J. Chem. Phys.* **2001**, *8*, 3540.
- Baer, R.; Neuhauser, D. *Phys. Rev. Lett.* **2005**, *94*, 043002.
- Yanai, T.; Tew, D. P.; Handy, N. C. *Chem. Phys. Lett.* **2004**, *393*, 51–57.
- Livshits, E.; Baer, R. *Phys. Chem. Chem. Phys.* **2007**, *9*, 2932–2941.
- Chiba, M.; Tsuneda, T.; Hirao, K. *J. Chem. Phys.* **2006**, *124*, 144106.
- Bylaska, E. J.; de Jong, W. A.; Govind, N.; Kowalski, K.; Straatsma, T. P.; Valiev, M.; Wang, D.; Apra, E.; Windus, T. L.; Hammond, J.; Nichols, P.; Hirata, S.; Hackler, M. T.; Zhao, Y.; Fan, P.-D.; Harrison, R. J.; Dupuis, M.; Smith, D. M. A.; Nieplocha, J.; Tipparaju, V.; Krishnan, M.; Wu, Q.; Van Voorhis, T.; Auer, A. A.; Nooijen, M.; Brown, E.; Cisneros, G.; Fann, G. I.; Fruchtl, H.; Garza, J.; Hirao, K.; Kendall, R.; Nichols, J. A.; Tsemekhman, K.; Wolinski, K.; Anshell, J.; Bernholdt, D.; Borowski, P.; Clark, T.; Clerc, D.; Dachsel, H.; Deegan, M.; Dyal, K.; Elwood, D.; Glendening, E.; Gutowski, M.; Hess, A.; Jaffe, J.; Johnson, B.; Ju, J.; Kobayashi, R.; Kutteh, R.; Lin, Z.; Littlefield, R.; Long, X.; Meng, B.; Nakajima, T.; Niu, S.; Pollack, L.; Rosing, M.; Sandrone, G.; Stave, M.; Taylor, H.; Thomas, G.; van Lenthe, J.; Wong, A.; Zhang, Z. *NWChem, A Computational Chemistry Package for Parallel Computers, Version 5.1*; Pacific Northwest National Laboratory: Richland, Washington 99352-0999, USA, 2007.
- (a) Hayden, L. M.; Sauter, G. F.; Ore, R. F.; Pasillas, P. L.; Hoover, J. M.; Lindsay, G. A.; Henry, R. A. *J. Appl. Phys.* **1990**, *88*, 456–465. (b) UV-vis spectrum of TCV in 1,2-dichloroethane was measured at the Army Research Laboratory.
- Isborn, C. M.; Leclercq, A.; Vila, F. D.; Dalton, L. R.; Bredas, J. L.; Eichinger, B. E.; Robinson, B. H. *J. Phys. Chem. A* **2007**, *111*, 1319–1327.
- Kinnibrugh, T.; Bhattacharjee, S.; Sullivan, P.; Isborn, C.; Robinson, B. H.; Eichinger, B. E. *J. Phys. Chem. B* **2006**, *110*, 13512–13522.



- (29) Leclercq, A.; Zojer, E.; Jang, S.-H.; Barlow, S.; Geskin, V.; Jen, A. K.-Y.; Marder, S. R.; Bredas, J. L. *J. Chem. Phys.* **2006**, *124*, 044510–044510.
- (30) Schmidt, K.; Barlow, S.; Leclercq, A.; Zojer, E.; Jang, S.-H.; Marder, S. R.; Jen, A. K.-Y.; Bredas, A.-L. *J. Mat. Chem.* **2007**, *17*, 2944–2949.
- (31) Frisch, M. J.; Trucks, G. W.; Schlegel, H. B.; Scuseria, G. E.; Robb, M. A.; Cheeseman, J. R.; Montgomery, J. A., Jr.; Vreven, T.; Kudin, K. N.; Burant, J. C.; Millam, J. M.; Iyengar, S. S.; Tomasi, J.; Barone, V.; Mennucci, B.; Cossi, M.; Scalmani, G.; Rega, N.; Petersson, G. A.; Nakatsuji, H.; Hada, M.; Ehara, M.; Toyota, K.; Fukuda, R.; Hasegawa, J.; Ishida, M.; Nakajima, T.; Honda, Y.; Kitao, O.; Nakai, H.; Klene, M.; Li, X.; Knox, J. E.; Hratchian, H. P.; Cross, J. B.; Bakken, V.; Adamo, C.; Jaramillo, J.; Gomperts, R.; Stratmann, R. E.; Yazyev, O.; Austin, A. J.; Cammi, R.; Pomelli, C.; Ochterski, J. W.; Ayala, P. Y.; Morokuma, K.; Voth, G. A.; Salvador, P.; Dannenberg, J. J.; Zakrzewski, V. G.; Dapprich, S.; Daniels, A. D.; Strain, M. C.; Farkas, O.; Malick, D. K.; Rabuck, A. D.; Raghavachari, K.; Foresman, J. B.; Ortiz, J. V.; Cui, Q.; Baboul, A. G.; Clifford, S.; Cioslowski, J.; Stefanov, B. B.; Liu, G.; Liashenko, A.; Piskorz, P.; Komaromi, I.; Martin, R. L.; Fox, D. J.; Keith, T.; Al-Laham, M. A.; Peng, C. Y.; Nanayakkara, A.; Challacombe, M.; Gill, P. M. W.; Johnson, B.; Chen, W.; Wong, M. W.; Gonzalez, C.; Pople, J. A. *Gaussian 03, Revision E.01*; Gaussian, Inc.: Wallingford, CT, 2004.
- (32) Lee, C. T.; Yang, W. T.; Parr, R. G. *Phys. Rev. B* **1988**, *37*, 785.
- (33) Becke, A. D. *J. Chem. Phys.* **1993**, *98*, 5648–5652.
- (34) Stephens, P. J.; Devlin, F. J.; Chabalowski, C. F.; Frisch, M. J. *J. Phys. Chem.* **1994**, *98*, 11623–11627.
- (35) (a) Tomasi, J.; Mennucci, B.; Cammi, R. *Chem. Rev.* **2005**, *105*, 2999–3094. (b) Cossi, M.; Scalmani, G.; Rega, N.; Barone, V. *J. Chem. Phys.* **2002**, *117*, 43.
- (36) Stratmann, R. E.; Scuseria, G. E.; Frisch, M. J. *J. Chem. Phys.* **1998**, *109*, 8218–8224.
- (37) Klamt, A.; Schuurmann, G. *J. Chem. Soc., Perkin Trans.* **1993**, *2*, 799.
- (38) Parr, R. G.; Yang, W. *Density-functional theory of atoms and molecules*; Oxford Univ. Press: Oxford, 1989.
- (39) Perdew, J. P.; Burke, K.; Ernzerhof, M. *Phys. Rev. Lett.* **1996**, *77*, 3865–3868.
- (40) (a) Ernzerhof, M.; Scuseria, G. E. *J. Chem. Phys.* **1999**, *110*, 5029–5036. (b) Adamo, C.; Barone, V. *J. Chem. Phys.* **1999**, *110*, 6158–6170.
- (41) Becke, A. *J. Chem. Phys.* **1993**, *8*, 1372–1377.
- (42) (a) Livshits, E.; Baer, R. *J. Phys. Chem. A* **2008**, *112*, 12789–12791. (b) Stein, T.; Kronik, L.; Baer, R. *J. Am. Chem. Soc.* **2009**, *131*, 2818.
- (43) Hirata, S.; Head-Gordon, M. *Chem. Phys. Lett.* **1999**, *314*, 291–299.
- (44) Dunlap, B. I.; Connolly, J. W. D.; Sabin, J. R. *J. Chem. Phys.* **1979**, *71*, 3396–3402.
- (45) Von Arnim, M.; Ahlrichs, R. *J. Comput. Chem.* **1998**, *19*, 1746–1757.
- (46) Godbout, N.; Salahub, D. R.; Andzelm, J.; Wimmer, E. *Can. J. Chem.* **1992**, *70*, 560–571.
- (47) Andrade do Monte, S.; Muller, T.; Dallos, M.; Lischka, H.; Diedenhofen, M.; Klamt, A. *Theor. Chem. Acc.* **2004**, *111*, 78–89.
- (48) Klamt, A.; Jonas, V.; Berger, T.; Lohrenz, J. C. W. *Phys. Chem. A* **1998**, *102*, 5074–5085.
- (49) Stefanovich, E. V.; Truong, T. N. *Chem. Phys. Lett.* **1995**, *244*, 65–74.
- (50) Schreiber, M.; Silva-Junior, M. R.; Sauer, S. P. A.; Thiel, W. *J. Chem. Phys.* **2008**, *128*, 134110.
- (51) Pearl, G. M.; Zerner, M. C.; Broo, A.; McKelvey, J. *J. Comput. Chem.* **1998**, *19*, 781–796.
- (52) Wong, B. M.; Cordaro, J. G. *J. Chem. Phys.* **2008**, *129*, 214703.
- (53) Rohrdanz, M.; Herbert, J. M. *J. Chem. Phys.* **2008**, *129*, 034107.
- (54) Peach, M. J. G.; Cohen, A. J.; Tozer, D. J. *Phys. Chem. Chem. Phys.* **2006**, *8*, 4543–4549.
- (55) Rohrdanz, M.; Martins, K. M.; Herbert, J. M. *J. Chem. Phys.* **2008**, *130*, 054112.
- (56) Peach, M. J. G.; Benfield, P.; Helgaker, T.; Tozer, D. J. *J. Chem. Phys.* **2008**, *128*, 044118.
- (57) Jacquemin, D.; Perpète, E. A.; Vydrov, O. A.; Scuseria, G. E.; Adamo, C. *J. Chem. Phys.* **2007**, *126*, 094102.

CT900231R